Catalog of Decaying Kink Oscillations of Coronal Loops in the 24th Solar Cycle

Alena Nechaeva[1,2] , Ivan V. Zimovets[1] , V. M. Nakariakov[3,4] , and C. R. Goddard[3]

[1] Space Research Institute (IKI), Russian Academy of Sciences, Profsoyuznaya St. 84/32, Moscow, 117997, Russia; nechaeva.ab@phystech.edu
[2] Moscow Institute of Physics and Technology, Institutskiy per. 9, Dolgoprudny, Moscow Region, 141701, Russia
[3] Centre for Fusion, Space and Astrophysics, Department of Physics, University of Warwick, CV4 7AL, UK
[4] St Petersburg Branch, Special Astrophysical Observatory, Russian Academy of Sciences, St Petersburg, 196140, Russia
Received 2018 December 26; revised 2019 February 19; accepted 2019 February 28; published 2019 April 12

Abstract

A catalog of kink oscillations of solar coronal loops, which spans during almost all of solar cycle 24, is presented. The catalog is based on the observations made in the extreme ultraviolet band at 171 Å with *Solar Dynamics Observatory*/Atmospheric Imaging Assembly and includes parameters of 223 oscillating loops in 96 oscillation events. The catalog provides the information about the oscillation locations, time, and dates of the events, associated flare, initial displacement, oscillation period, exponential damping time, and apparent amplitude. The vast majority of the oscillation detections, 84%, were made in the loops situated near or off the solar limb. The oscillation periods are found to range from 1 to 28 minutes, with 74% of the events that have the period in the range of 2–10 minutes. About 90% of the oscillations have the apparent amplitude in the range of 1–10 Mm. The oscillating loop lengths are 70–600 Mm. The typical apparent amplitude is about 1% of the loop length. The oscillation period scales linearly with the loop length, and the damping time scales linearly with the period, which confirm previous findings. The oscillation quality factor scales with the amplitude to the power of minus 0.7. No statistically significant evidence of correlation was found between both the oscillation period and the mean sunspot number, and the loop length and mean sunspot number. The catalog provides the research community with the foundation for the further statistical study of kink oscillations and their use for coronal seismology.

Key words: Sun: activity – Sun: corona – Sun: oscillations

Supporting material: machine-readable table

1. Introduction

Transverse oscillations of solar coronal loops, usually called kink oscillations, are one of the most studied oscillatory phenomena in the solar corona. Their existence was predicted in the seminal works of Zajtsev & Stepanov (1975) and Roberts et al. (1984), as standing fast magnetoacoustic waves of the $m = 1$ symmetry.

Kink oscillations were discovered with the use of the narrowband high-resolution extreme ultraviolet imager Transition Region and Coronal Explorer (TRACE; Aschwanden et al. 1999; Nakariakov et al. 1999), and for several years remained a rather exotic phenomenon with only several observational detections. However, the unexpectedly rapid decay of those oscillations stimulated a number of theoretical studies, resulting in major progress of our understanding of the interaction of magnetohydrodynamic (MHD) waves with plasma nonuniformities (e.g., Ruderman et al. 2008). In addition, kink oscillations became a popular tool for MHD seismology of the coronal plasma, providing unique diagnostics of the absolute value of the magnetic field in the oscillating loop (e.g., Nakariakov & Ofman 2001; Chen & Peter 2015) and giving information about the transverse profile of the plasma density (e.g., Goddard et al. 2018), density stratification (e.g., Andries et al. 2005, 2009), and the variation of the Alfvén speed along the loop (e.g., Ruderman et al. 2008).

Attempts to establish intrinsic features of kink oscillations by a statistical analysis of available events were carried almost since the discovery of this phenomenon. Aschwanden et al. (2002) analyzed the first 27 detected kink oscillation events, observed with TRACE, and found out that their periods, wavelengths, and amplitudes have broad distributions. Ofman & Aschwanden (2002) established that the damping time scales linearly with the oscillation period, which indicated that the effect of resonant absorption is the preferential mechanism for the kink oscillation damping. This finding was later confirmed by, e.g., Verwichte et al. (2013). Aschwanden et al. (2003) seismologically estimated the average ratio of the densities inside and outside oscillating loops and demonstrated that the observed period-damping time scaling law does provide information about the physical damping mechanism.

Major progress in the observational detection of kink oscillations was achieved by the commissioning of the Atmospheric Imaging Assembly on board the *Solar Dynamics Observatory* (*SDO*/AIA Lemen et al. 2012), which dramatically increased the number of detected events, improved the estimation of the oscillation parameters, and provided the ground for the comprehensive statistical study of this phenomenon. Zimovets & Nakariakov (2015) compile the first comprehensive catalog of kink oscillations detected during the first four years of the *SDO*/AIA operation (2010–2014). The catalog included information about 169 different oscillating loops, with their location and oscillation times; the start and peak times and the location of the associated flare X-ray emission; the start times and locations of the associated low coronal eruptions; and the information about the associated type-II radio bursts. The use of this catalog established that, in the vast majority of cases, kink oscillations are excited by a mechanical displacement caused by a low coronal eruption.

Later on, Goddard et al. (2016) added information about the initial apparent amplitude, period, length of the oscillating loop, and damping times of the oscillating loops to the catalog. This allowed the authors to establish that the oscillation period scales linearly with the loop length, which confirmed the

interpretation of the kink oscillation phenomenon in terms of standing fast magnetoacoustic waves. The initial loop displacement was found to prescribe the initial amplitude of oscillation. In addition, the damping time scales linearly with the oscillation period was confirmed, while those two parameters are strongly scattered.

Goddard & Nakariakov (2016) used the catalog for the determination of an empirical dependence of the kink oscillation damping time and its quality factor, which revealed the nonlinear nature of the damping process. This recent finding has already stimulated a number of theoretical studies addressing the nonlinear regime of kink oscillations (e.g., Magyar & Van Doorsselaere 2016; Hillier et al. 2019).

The aim of this work is provide the research community with a major extension of the kink oscillation catalog, covering almost the whole 24th solar cycle. This catalog can be used as a basis for conducting more detailed studies of various aspects of the decaying kink oscillations of coronal loops. In this work, we restricted ourselves to analyzing distributions and statistical correlations of only the main parameters of oscillations (such as loop length, oscillation period, initial loop displacement and oscillation amplitude, and damping time, where it is possible to measure).

2. Data Analysis

In the previous work (Goddard et al. 2016), 48 kink oscillation events, including 120 individual loop oscillations, were analyzed with the use of SDO/AIA data in 171 Å, obtained from 2010 May 20 (when SDO/AIA data became available) to 2014 May 20. In this work, we significantly extend the catalog by adding the data that span from 2014 May 20 to 2018 December 26. To create this catalog, the oscillation events found via the Heliophysics Events Knowledgebase[5] were checked for the time span from 2014 May 20 to 2018 December 26. In addition, the time interval from 2017 August 1 to October 31, including the period of high solar activity in the beginning of 2017 September, was looked through manually using JHelioviewer[6] (Müller et al. 2017). We found 52 new events, but the analysis for 4 of them was not possible. In the end, 48 new events were analyzed and included in the final catalog, containing 96 oscillating loops. The new catalog covers almost the entire 24th solar cycle. Since the activity of the Sun is at a very low level and is close to a minimum on the day of the submission of this work, and as there are already magnetic elements of the polarity corresponding to the new 25th cycle, new oscillation events associated with low coronal eruptions and flares (Hudson & Warmuth 2004; Zimovets & Nakariakov 2015) and belonging to Cycle 25 are unlikely. Even if they happen, there will be very few of them, which should not affect the results of the statistical analysis presented here.

We requested 1500 SDO/AIA 171 Å image frames with the time step of 12 s (in most of cases) for each event, using SolarSoftWare,[7] and the files were downloaded for a further analysis. The procedure of creating time–distance (TD) maps of kink oscillations of coronal loops is described in (Goddard et al. 2016). Linear slits of 5 pixels in width are taken perpendicular to each oscillating loop near its apex (in most
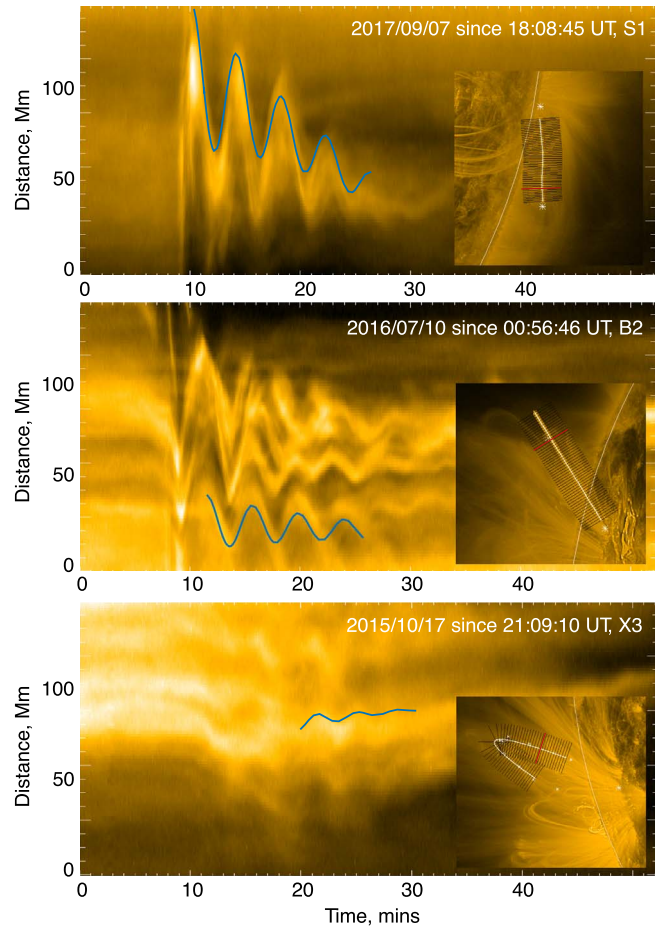

Figure 1. Examples of the TD maps of kink oscillations of three different types: S1, B2, and X3 (from top to bottom, respectively), as described in Section 2. The blue curves show best-fitting exponentially decaying harmonic signals with power-law trends. The inset shows the active region with loops, and the red line corresponds to the slit shown.

cases), and then the intensities along the slits are stacked in time, creating the TD maps. Examples of TD maps are shown in Figure 1. Coordinates of the slit endpoints are listed in Table 1. Figure 2 visualizes the spatial distribution of the centers of each slit on the solar disk. One can see in Figure 2 that the majority of the events selected, 84%, happened off the solar limb. This just indicates that it is easier to identify and analyze oscillations above the limb, against the background of a dark sky, than against the background of the bright solar disk.

The length of each loop is estimated under the assumption that the loops are close to the semicircular shape, by either measuring the projected distance between the footpoints or by the apparent height. The loop lengths are listed in Table 1. Errors were obtained by a process of repeating measurements, taking the standard deviation of obtained loop lengths as the error. No other errors, such as errors from the line of sight (LoS) or uncertainty in coordinates of loop footpoints if they are behind the limb, were taken into account.

Automatic loop tracking is not performed due to the time-consuming nature of implementing a reliable algorithm to obtain the oscillatory signal of each loop of interest and the absence of robust algorithms. Thus, locations of the boundaries of oscillating loops were determined by eye. An example of TD map with dots picked to track the oscillation is shown in

3

Table 1
Parameters of 223 Decaying Kink Oscillations of Coronal Loops Detected with *SDO*/AIA at 171 Å in 2010–2018

Event ID	Loop ID	LC	Slit Position [x1, x2, y1, y2], arcsec	Date	Time UT	Flare	Period minutes	Length Mm	Init. Disp. Mm	Osc. Amp. Mm	Damping Time minutes
1	1	S2	−940, −964, −321, −308	2010 Aug 2	04:22:49	SOL2010-08-02T4:20	3.42 ± 0.06	232	5.1	1.7	5.34 ± 1.12
1	2	B2	−962, −997, −313, −322	2010 Aug 2	04:22:13	SOL2010-08-02T4:20	4.11 ± 0.05	78	7.0	1.2	10.76 ± 2.79
2	1	S1	672,711, −259, −223	2010 Oct 12	19:13:07	⋯	6.64 ± 0.06	156	2.0	4.8	⋯
3	1	S1	−977, −988, −383, −368	2010 Nov 3	12:13:48	SOL2010-11-0T12:12	2.46 ± 0.03	213	1.4	4.7	8.8 ± 1.8
3	2	S2	−970, −1001, −416, −393	2010 Nov 3	12:14:35	SOL2010-11-03T12:12	3.62 ± 0.08	262	4.4	9.7	4.12 ± 0.47
3	3	S3	−978, −1027, −466, −411	2010 Nov 3	12:14:23	SOL2010-11-03T12:12	4.04 ± 0.1	311	4.1	8.9	⋯
4	1	S1	912, 889, 405, 433	2011 Feb 9	01:30:02	SOL2011-02-09T01:26	2.29 ± 0.03	183	2.9	4.4	7.18 ± 1.5
4	2	X3	969, 974, 231, 278	2011 Feb 9	01:31:54	SOL2011-02-09T01:26	3.47 ± 0.03	181	1.4	1.2	7.44 ± 1
5	1	S1	1089, 1050, 375, 423	2011 Feb 10	04:43:38	SOL2011-02-10T04:43	7.03 ± 0.06	438	4.5	3.0	⋯
6	1	B3	1089, 1057, 349, 398	2011 Feb 10	06:44:22	SOL2011-02-10T06:38	8.05 ± 0.26	430	3.8	0.5	⋯
⋮	⋮	⋮	⋮	⋮	⋮	⋮	⋮	⋮	⋮	⋮	
49	1	S2	−1117, −1069, −345, −309	2014 Jun 10	11:39:47	SOL2014-06-10T11:36	8.52 ± 1.02	411 ± 10	1.6	3.7 ± 1.7	8.6 ± 3.6
50	1	B2	−1039, −1020, −139, −196	2014 Jun 10	12:43:25	SOL2014-06-10T12:35	7.36 ± 0.26	313 ± 36	4.3	2.5 ± 0.6	24.8 ± 12.1
50	2	B2	−1111, −1067, −169, −210	2014 Jun 10	12:43:25	SOL2014-06-10T12:35	12.60 ± 1.02	358 ± 10	24.0	19.9 ± 7.1	⋯
50	3	X3	−1041, −1004, −153, −200	2014 Jun 10	12:43:25	SOL2014-06-10T12:35	8.34 ± 1.49	238 ± 10	1.9	2.5 ± 1.0	⋯
51	1	S2	−1082, −1056, −495, −441	2014 Jun 11	08:05:25	SOL2014-06-11T08:00	22.76 ± 1.85	485 ± 11	6.6	18.3 ± 4.0	⋯
51	2	B2	−1093, −1047, −389, −426	2014 Jun 11	08:05:25	SOL2014-06-11T08:00	13.75 ± 0.38	451 ± 10	5.5	6.8 ± 1.5	23.2 ± 8.9
52	1	B2	−1072, −1027, −383, −423	2014 Jun 11	09:01:47	SOL2014-06-11T08:59	13.51 ± 0.42	448 ± 11	2.6	4.1 ± 0.8	27.3 ± 11.1
52	2	B2	−1086, −1026, −460, −458	2014 Jun 11	09:01:47	SOL2014-06-11T08:59	12.95 ± 0.73	423 ± 11	10.0	5.8 ± 1.5	15.6 ± 4.4
52	3	X2	−1096, −1044, −333, −363	2014 Jun 11	09:01:47	SOL2014-06-11T08:59	9.38 ± 0.26	397 ± 9	1.2	2.0 ± 0.5	⋯
52	4	B3	−1019, −984, −530, −481	2014 Jun 11	09:01:47	SOL2014-06-11T08:59	25.85 ± 1.79	403 ± 14	4.4	5.3 ± 0.9	⋯

Note. The table gives the event number, loop number in the event, loop class, coordinates of slit position, event's date and starting time, information about the associated flare determined by *GOES*, oscillation period, loop length, initial displacement, and oscillation amplitude and damping time, where it was possible to measure.

(This table is available in its entirety in machine-readable form.)
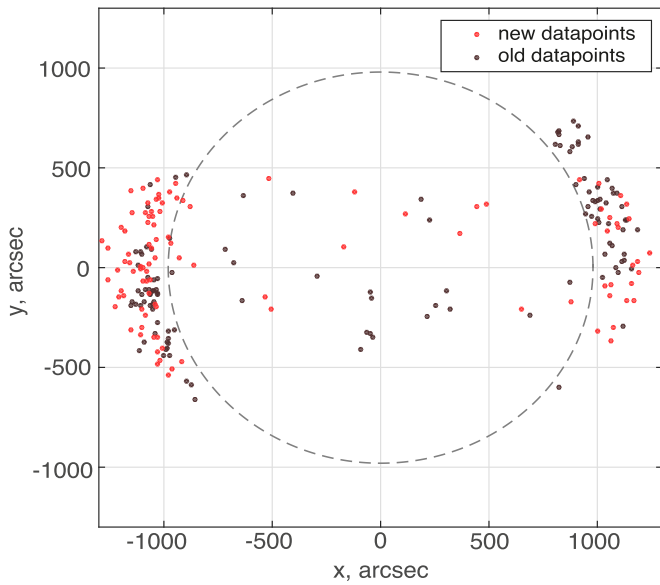
Figure 2. Locations of the centers of each slit used in the analysis of kink oscillations on the solar disk. The dark brown dots correspond to the data from Goddard et al. (2016), and the red dots correspond to the new data.
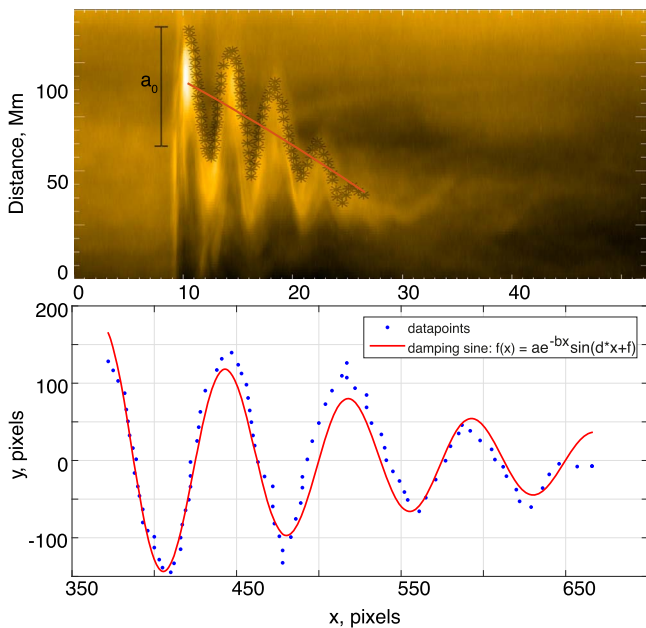

Figure 3. Example of the determination of the oscillation parameters. (Top panel): the semi-transparent black stars show the instantaneous positions of the boundary of the oscillating loop, picked by hand for tracking the oscillation. The power-law background trend is shown by the red line. The initial displacement a_0 is also shown. (Bottom panel): the blue dots show the detrended signal. The red curve shows the best-fitting exponentially decaying harmonic oscillation.

Figure 3 (top panel). The initial displacement a_0 was estimated as the distance between the initial position of the loop and the top of the first peak.

The background trend was determined by best fitting a power-law to the oscillatory signal, which was then subtracted from the data. The detrended signal was approximated by an exponentially damped sine function $F(t) = a\exp(-t/\tau)\sin(2\pi t/P + C)$, where the constants P,

τ, and C are the oscillation period, exponential damping time, and initial phase, respectively. All the fittings were performed with the use of the `fittype` function of Matlab, which uses the nonlinear least squares method. An example is shown in Figure 3 (bottom panel). Testing revealed no significant difference between this method and performing the background and oscillatory fits together, so the detrending approach is chosen to limit the number of free parameters in the fitting. For the determination of amplitude[8] A of the oscillation, first periods of detrended signal were fitted with sine function $F(t) = (A/2)\sin(2\pi t/P + c)$. The parameters A, P, τ, and C were determined with their errors.

All the oscillations were divided in three groups based on the types of loops observed and in three groups based on the data quality. It is provided to aid future users of the catalog in selecting events for further study. Three groups based on the type of loops are segment, where we can clearly see a part of loop that does not interfere with other loops; bundle, where there are several parallel loops; and crossing, where there are several other loops crossing the analyzed loop. These groups are marked as S, B, and X, respectively. One can distinguish S from B on TD maps. The S case is when the distance between individual loops on the TD map is bigger than the amplitudes of their oscillations, and the B case when the distance between individual loops on the TD map is smaller than the amplitudes of their oscillations. There are also three groups based on the quality of data. A data quality of 1 corresponds to a clearly observed oscillation of a loop or bundle with a clearly defined edge and/or center, and the data is considered promising for future study, such as seismological applications. A data quality of 2 reflects lower-quality data, where part of the oscillation or structure is obscured and/or the data is noisy, but may still provide useful information for future study. A data quality of 3 corresponds to low-quality data, where any measurement beyond a period estimate is very subjective. The class of the loop is described by the letter and the number, which specifies the type of the loop and the quality of the data in Table 1, e.g., S2. Examples of several loops corresponding to different classes are shown in Figure 1. Note that this categorization is made for the slit positions reported, which should be considered as the preliminary and quite subjective categorization.

The error in the damping time τ is rather high due to the small number of the detected oscillation cycles. In addition, the damping profiles in our analysis were assumed to be exponential, and we neglect the possibility of either Gaussian damping, or a combination of the Gaussian and exponential damping profiles, as suggested by Pascoe et al. (2013, 2016). However, distinguishing between different regimes of damping and determination of the best-fitting parameters is a laborious task that requires time-consuming techniques, such as the Markov chain Monte Carlo sampling (e.g., Pascoe et al. 2017). Thus, the approximation of the damping profile by an exponential function, performed in this study, could be considered as a zero-order approximation only and should be extended in a more detailed analysis of the statistics of the kink oscillation damping. Parameters of the oscillations are summarized in Table 1.

Table 1 gives loop class, as described earlier; the coordinates of slit positions; the events' dates and starting times; the

---

[8] This choice of the amplitude was made to make our analysis consistent with the definition used in Goddard et al. (2016)
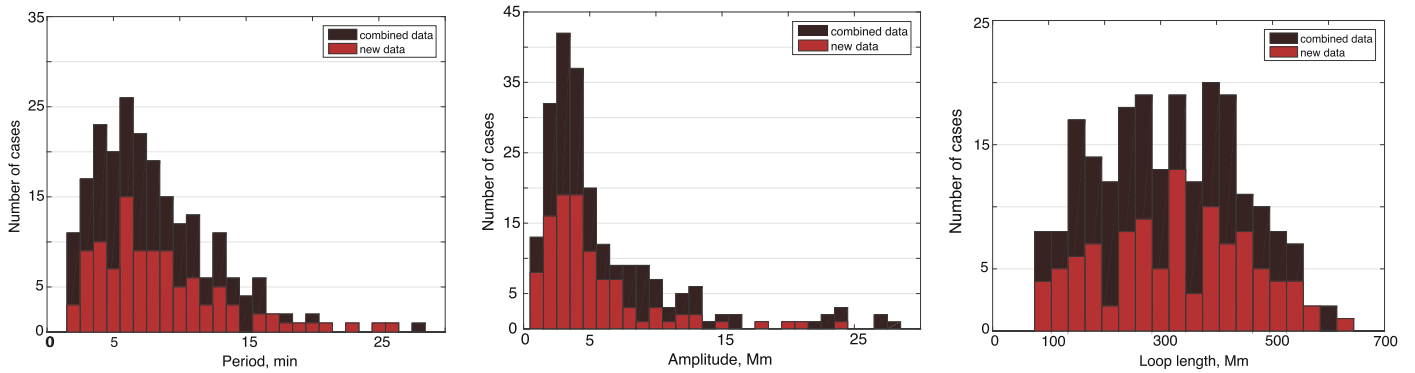
Figure 4. Distribution of kink oscillation parameters, determined for 223 oscillating loops. (Left panel): the measured periods of oscillating loops analyzed. The bin size is 1 min. (Center panel): the measured oscillation amplitudes. The bin size is 1 Mm. (Right panel): the measured loop lengths. The bin size is 30 Mm.

information about the associated flares determined by the *Geostationary Operational Environmental Satellite* (*GOES*); the oscillating loop lengths; the oscillation periods; the apparent oscillation amplitudes; the damping times; and the initial displacements. Below, we present the results obtained by the preliminary analysis of the catalog.

3. Results

Considering both old and new events, the oscillation periods were determined in 223 cases, the lengths of the oscillating loops were determined in 221 cases, the displacement and oscillation amplitude were determined in 223 cases, and the damping time were determined in 101 cases. Below, we summarize the results obtained by the analysis of the extended catalog.

The Kolmogorov–Smirnov test of all the parameters was done with the use of the `kstest2` function of Matlab, which tested two vectors of data: the first one obtained by Goddard et al. (2016) and the second one in this study for each parameter. The test does not reject the null hypothesis (that the vectors of data are from the same continuous distribution) at the 1% significance level for each parameter. Therefore, we consider the measured parameters in both halves of the catalog to belong to the same statistics, despite the slightly different methodology used.

It should be mentioned that in this study, we use the Pearson correlation coefficient as the data clouds are moderately scattered, and examination of nonlinear relationships between the parameters should be the subject of further study.

3.1. Histograms of the Oscillation Parameters

The histograms were made for the oscillation period *P*, amplitude *A*, and loop length *L* (Figure 4). The measured oscillation periods are found to range from 1 to 28 minutes. Periods range from 2–10 minutes for 74% of the events. Long-period oscillations are found to be rather rare. The majority of the events are found to have periods shorter than 5–7 minutes. The apparent, i.e., projected on the plane of the sky, amplitudes range from 1–10 Mm for 90% of the oscillations. The peak of the distribution is between 2 and 4 Mm. Most of the loops analyzed have lengths in the range of 150–420 Mm, which is 22%–60% of the solar radius. From this finding, we can conclude that we deal mainly with (1) quite large-scale coronal loops (Reale 2014), and (2) the low amplitude oscillations with the average amplitude of about 1% of the loop length. The first

circumstance seems to be related to the observational bias: it is easier to find long oscillating loops than short ones.

3.2. Dependence of the Oscillation Period on the Loop Length

In Figure 6 (left top panel), the oscillation periods are plotted against the oscillating loop lengths. The linear correlation coefficient between these two parameters is 0.661 (95% confidence bounds: [0.579; 0.729]). The unweighted linear fit, $P/\text{minutes} = a_{\text{PL}}(L/\text{Mm})$, was implemented to the data, which gave $a_{\text{PL}} = 0.025 \pm 0.001$. This parameter results in the kink speed of $C_k = 1328 \pm 53\,\text{km s}^{-1}$, which can be calculated from the equation $P = 2L/C_k$. The obtained value of the kink speed coincides, within the measurement errors, with the value found in Goddard et al. (2016) for the twice smaller sample of oscillating events. This result is in a good agreement with the theory of kink oscillations of coronal loops. The apparent increase in the oscillation period with the loop length, i.e., a possible departure of the scaling from linear for longer loops, could be attributed to the effect of the expansion of the loop cross section with height. This effect would require a dedicated study.

3.3. Dependence of the Oscillation Amplitude on the Initial Displacement

In Figure 5 (right top panel), the amplitude of the oscillations is plotted against the initial displacement of the oscillating loops. The linear correlation coefficient between these two parameters is 0.596 (95% confidence bounds: [0.504; 0.675]). This amplitude–displacement scatter plot is an extended version of the plot shown in Figure 6 in Goddard et al. (2016).

3.4. Dependence of the Oscillation Amplitude on the Loop Length

In Figure 5 (left bottom panel), the amplitude of the oscillations is plotted against the length of the oscillating loops. The linear correlation coefficient between these two parameters is 0.431 (95% confidence bounds: [0.317; 0.533]). However, since the correlation coefficient is quite small, we cannot make a reliable conclusion. This question requires further study.
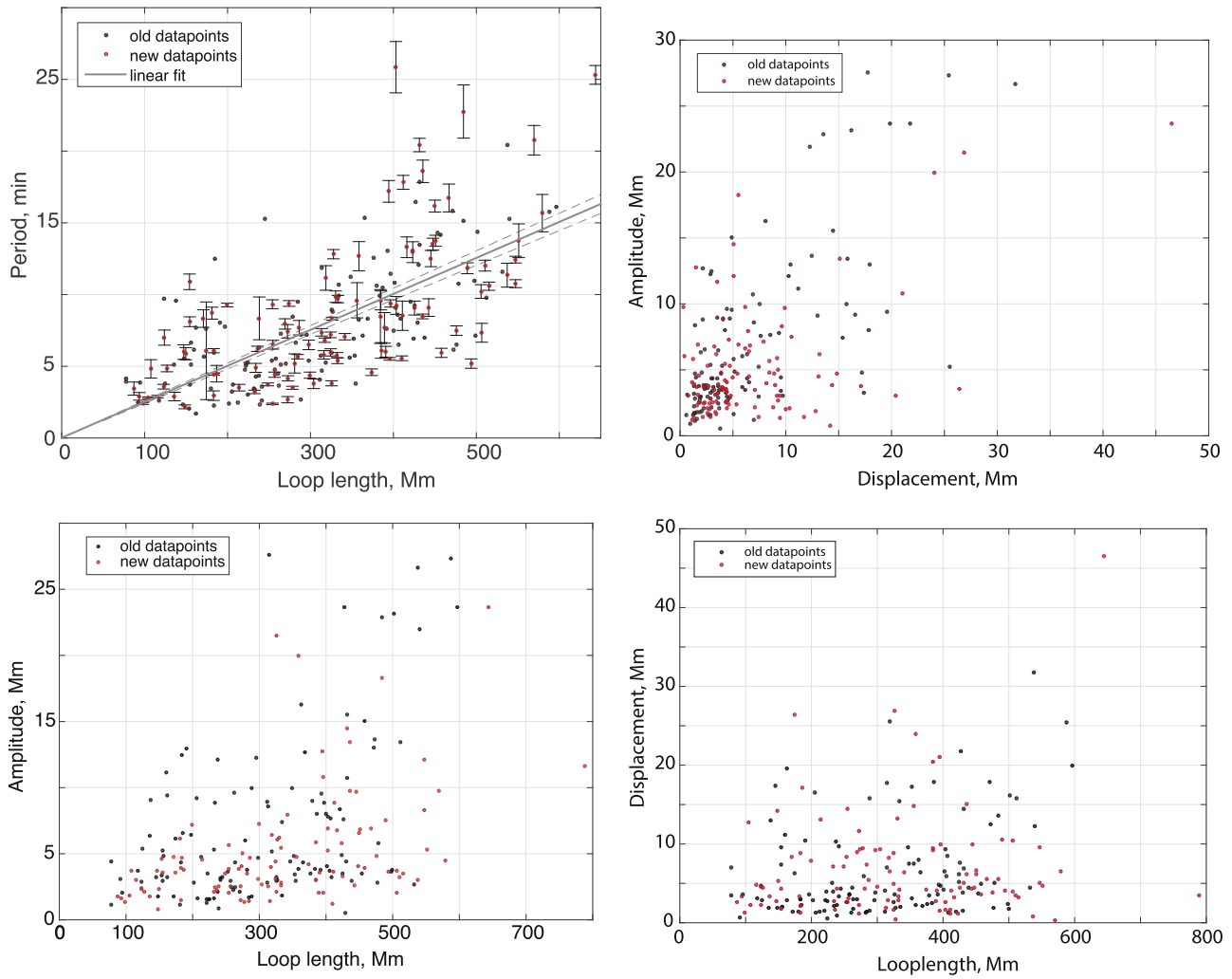
Figure 5. Mutual scalings of parameters of 223 kink oscillations. (Top left): periods against the oscillating loop lengths. The linear fit of the data passing through the origin is shown by the solid gray line with a gradient of 0.025 ± 0.001. The gradient error is shown by the gray dashed lines. (Top right): apparent oscillation amplitudes against the initial loop displacement. (Bottom left): apparent oscillation amplitudes against the loop lengths. (Bottom right): initial displacement against the loop length.

3.5. Dependence of the Oscillation Initial Displacement on the Loop Length

In Figure 5 (right bottom panel), the initial displacement of the oscillating loops is plotted against their length. The linear correlation coefficient between these two parameters is only 0.213 (95% confidence bounds: [0.083; 0.335]), because the linear (or any other) fit of the data cloud is not presented. From this, we can conclude that the initial displacement of the loop is almost independent of its length.

3.6. Dependence of the Oscillation Damping Time on the Loop Length

It is possible to determine the damping time only for 101 oscillating loops because of the data limitations related, in particular, to the small number of observed oscillation cycles or an unclear damping function that is different from the exponential one.

In Figure 6 (left top panel), the damping time of 101 oscillations is plotted against the oscillating loop length. The linear correlation coefficient between these two parameters is found to be 0.533 (95% confidence bounds: [0.378; 0.659]).

The linear fit of $\tau/\text{minutes} = a_{\tau A}(A/\text{Mm})$ was used, which gave $a_{\tau A} = 0.049 \pm 0.001$. Thus, there is some evidence that the oscillation damping time can be linearly proportional to the loop length. This is expected due to the scaling of period with loop length and the dependence of the damping time on period.

3.7. Dependence of the Oscillation Damping Time on the Oscillation Period

In Figure 6 (right top panel), the damping time of 102 oscillations is plotted against the oscillation period. The linear correlation coefficient between these two parameters is 0.640 (95% confidence bounds: [0.508; 0.742]). The linear fit of $\tau/\text{minutes} = a_{\tau P}(P/\text{minutes})$ was used, which gave $a_{\tau P} = 1.79 \pm 0.14$. Thus, the oscillation damping time may depend linearly on the oscillation period that confirms the previous estimations of this scaling, based on smaller data sets (Aschwanden et al. 2002; Verwichte et al. 2013; Goddard et al. 2016).
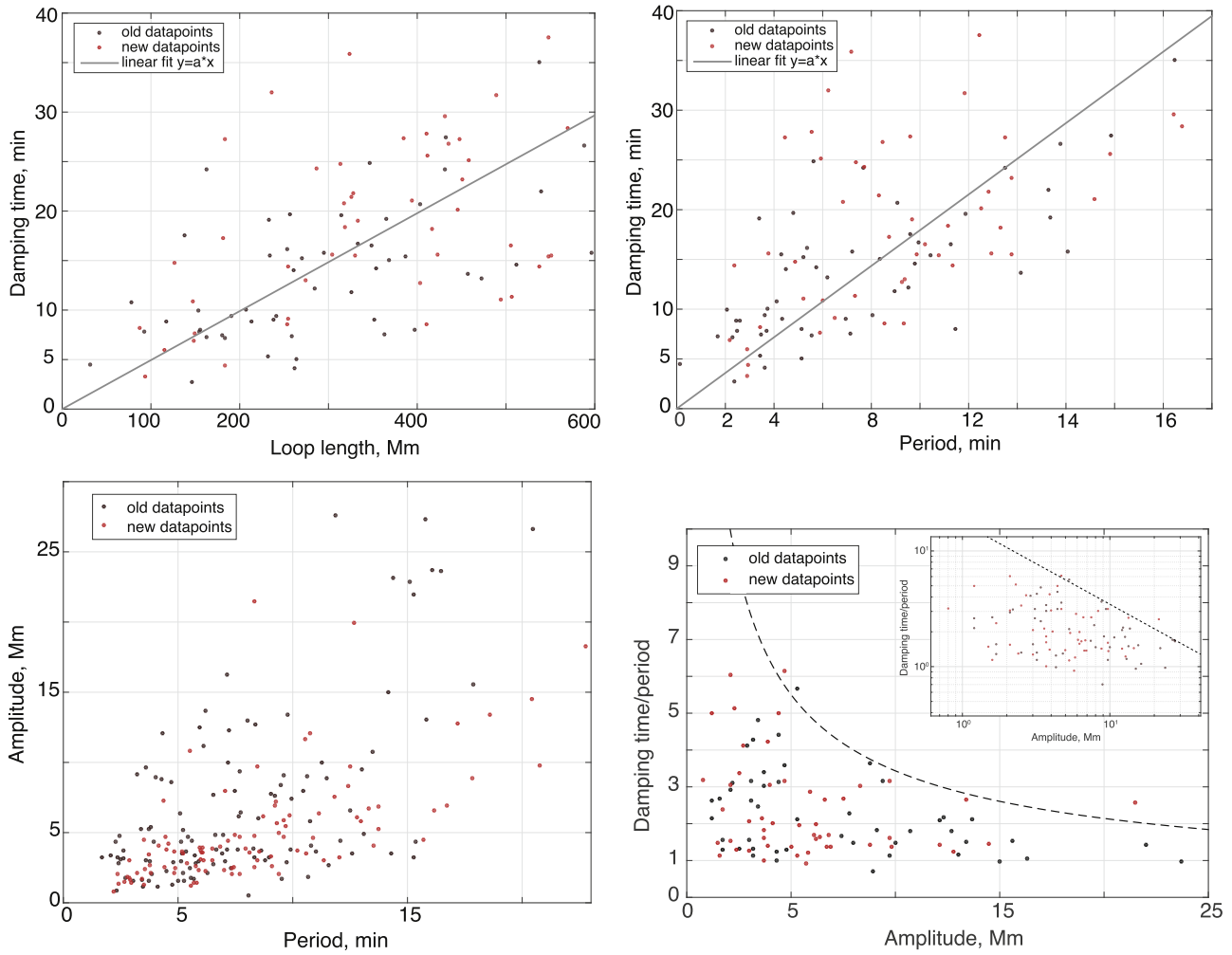
Figure 6. (Top left): damping time of 101 kink oscillations of coronal loops plotted against the loop length. The linear fit of the data passing through the origin is shown by the solid gray line with a gradient of 0.049 ± 0.001. (Top right): damping time of 101 kink oscillations of coronal loops plotted against the period. The linear fit of the data passing through the origin is shown by the solid gray line with a gradient of 1.79 ± 0.14. (Bottom left): the apparent amplitude of 221 kink oscillations of coronal loops plotted against the period. (Bottom right): quality factor of 101 kink oscillations of coronal loops plotted against the oscillation amplitude. The inset shows the same dependence in the log–log plot. The dotted and dashed curves show the approximation of the upper-right boundary of the data clouds with a linear function in the log–log plot and the corresponding power-law function in the linear plot, respectively.

3.8. Dependence of the Oscillation Amplitude on the Period

In Figure 6 (left bottom panel), the oscillation amplitude is plotted against the oscillation period. The linear correlation coefficient between these two parameters is 0.579 (95% confidence bounds: [0.484; 0.661]).

3.9. Connection between the Quality Factor of the Oscillations and Their Amplitude

In Figure 6 (right top panel), the quality factor Q, defined as the ratio of the damping time to the period, is plotted against the oscillation amplitude. The same data is presented in the inlet in the log–log scale. The scatter plot shown in Figure 6 (right top panel) is similar to the plot shown in Figure 2 in Goddard et al. (2016). The only difference is the increased number of data points presented. The plot demonstrates that, in general, larger amplitudes correspond to smaller quality factors of the oscillations. The explanation of the apparent triangular shape of the data point cloud (in the linear scale) was given in Goddard et al. (2016). This triangular shape is due to the fact that we did not measure the real amplitude of oscillations, but the apparent amplitude perpendicular to the LoS, because of the

fact that the loops were oriented in an arbitrary way relative to the LoS. The approximation of the upper-right outer boundary of the data cloud in the log–log plot by a linear function gives $\log Q \approx -(0.68 \pm 0.13)\log(A/\mathrm{Mm}) + (2.80 \pm 0.37)$. Thus, the quality factor scales as $A^{-0.7}$. This result demonstrates the need for determination of this dependence from theoretical models, allowing for their validation.

3.10. Time Dependencies of the Oscillation Parameters with the Course of the Solar Cycle

The time period considered, 2010–2018, covers almost the whole 24th solar cycle. Thus, we can try to investigate the variation of the parameters of the studied oscillations with the course of the solar cycle. In Figure 7, the time evolution of the oscillation period, P, and the length of the oscillating loops, L, in the course of the solar cycle are shown.

The solar cycle is divided into two parts: the rise phase (before winter 2013–14) and the decline phase (after winter 2013–14). The linear correlation coefficients for these two pairs of signals are 0.673 (95% confidence bounds: [0.246; 0.882]) and 0.566 (95% confidence bounds: [0.076; 0.836]),
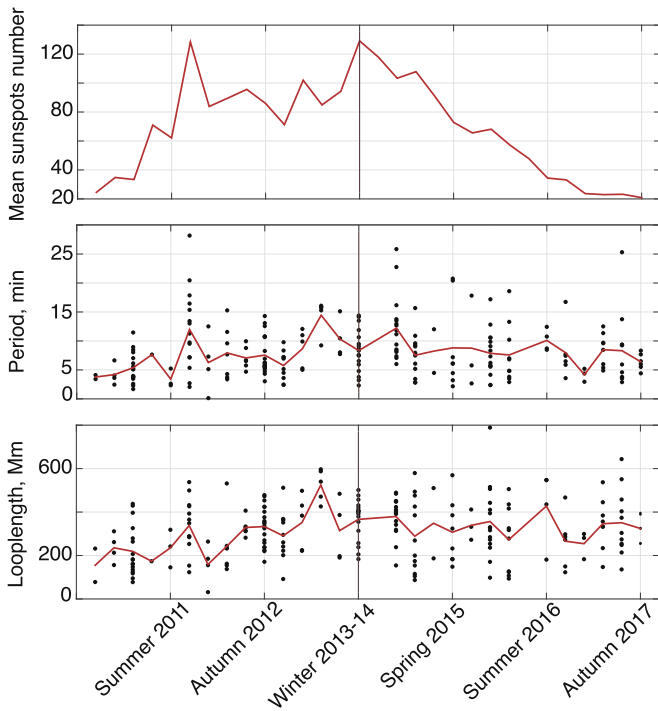
Figure 7. (Top panel): the average sunspot number. Thick vertical line separates the rising and declining phases of the solar cycle. (Center panel): time evolution of the detected oscillation periods and (Bottom panel): the oscillating loop lengths (central) from 2010 August to 2017 October. The black data points correspond to the measured periods of the oscillations. The red curve corresponds to the evolution of the mean value. The time step is 3 months.

respectively. In the decline phase, the corresponding correlation coefficients are smaller: 0.443 (95% confidence bounds: [−0.143; 0.799]) and 0.082 (95% confidence bounds: [−0.490; 0.606]), respectively. The large confidence bounds on these correlation coefficients means we have no evidence for correlations between the loop length or period and the mean sunspot number in either phase. We acknowledge limitations in our current analysis, and a more detailed statistical analysis should be the subject of further work.

The linear correlation coefficient for the kink speed and the sunspot number averaged over a time span of three months is −0.337 (95% confidence bounds: [−0.724; 0.212]) and −0.504 (95% confidence bounds: [−0.826; 0.064]) for the rising and declining phases of the solar cycle, respectively. Such small values of the correlation coefficient with such large errors do not allow us to make any certain conclusions about the presence of the correlation or anti-correlation between these two physical quantities. This would require a more detailed analysis and/or extension of statistics.

4. Conclusion

A comprehensive catalog of decaying kink oscillations of solar coronal loops detected with SDO/AIA at 171 Å from 2010 May 20 to 2018 December 26, and thus covering (almost) the entire 24th solar cycle, is created. The catalog extends the catalog presented in Zimovets & Nakariakov (2015) and Goddard et al. (2016), almost doubling the number of oscillating loops. The catalog contains the following information for 223 oscillating loops in 96 events: the starting date and time of oscillation event, information about an accompanying flare event, number of oscillating loops identified, slit

coordinates used for the analysis, oscillation period, loop length, initial displacement amplitude, oscillation amplitude, and damping time (where it was possible to measure) with the rough estimations of the errors of these physical parameters.

Based on the simple analysis of the information presented in the new catalog, we obtained the distributions of the main parameters of oscillating loops and their dependencies on each other. The specific results obtained are:

1. The period scales linearly with the loop length, as expected, and the average kink speed is $C_k = 1328 \pm 53$ km s^{-1}. This finding strengthens the conclusion drawn in Goddard et al. (2016), confirming that kink oscillations are natural modes of coronal loops.
2. The initial oscillation amplitude depends on the initial loop displacement.
3. The linear correlation between the damping time and the loop length, and between the damping time and oscillation period, is confirmed. This scaling is the foundation of the interpretation of the kink oscillation damping in terms of the resonant absorption mechanism (e.g., Goossens et al. 2002; Ofman & Aschwanden 2002; Ruderman & Roberts 2002).
4. A systematic decrease of the ratio of the damping time to the oscillation period, i.e., the oscillation quality, with the oscillation amplitude is confirmed; the quality factor is found to scale as the oscillation amplitude to the power of minus 0.7. This result quantifies the qualitative finding of Goddard & Nakariakov (2016). This scaling should be taken into account in the studies of nonlinear resonant absorption.
5. No statistically reliable evidence of correlation between the oscillating loop length and the mean sunspot number, and oscillation period and the mean sunspot number, was found. This result could indicate that a more precise study of the evolution of the average parameters of kink oscillations with the solar cycle is needed and may have important seismological implications.

The catalog creates a representative ground for specialized studies of various aspects of the decaying kink oscillations of coronal loops and coronal seismology.

ORCID iDs

Alena Nechaeva ⓘ https://orcid.org/0000-0002-3549-3015
Ivan V. Zimovets ⓘ https://orcid.org/0000-0001-6995-3684
V. M. Nakariakov ⓘ https://orcid.org/0000-0001-6423-8286
C. R. Goddard ⓘ https://orcid.org/0000-0003-0240-0465

References

Andries, J., Arregui, I., & Goossens, M. 2005, ApJL, 624, L57
Andries, J., van Doorsselaere, T., Roberts, B., et al. 2009, SSRv, 149, 3
Aschwanden, M. J., de Pontieu, B., Schrijver, C. J., & Title, A. M. 2002, SoPh, 206, 99

Aschwanden, M. J., Fletcher, L., Schrijver, C. J., & Alexander, D. 1999, ApJ, 520, 880

Aschwanden, M. J., Nightingale, R. W., Andries, J., Goossens, M., & Van Doorsselaere, T. 2003, ApJ, 598, 1375

Chen, F., & Peter, H. 2015, A&A, 581, A137

Goddard, C. R., Antolin, P., & Pascoe, D. J. 2018, ApJ, 863, 167

Goddard, C. R., & Nakariakov, V. M. 2016, A&A, 590, L5

Goddard, C. R., Nisticò, G., Nakariakov, V. M., & Zimovets, I. V. 2016, A&A, 585, A137

Goossens, M., Andries, J., & Aschwanden, M. J. 2002, A&A, 394, L39

Hillier, A., Barker, A., Arregui, I., & Latter, H. 2019, MNRAS, 482, 1143

Hudson, H. S., & Warmuth, A. 2004, ApJL, 614, L85

Lemen, J. R., Title, A. M., Akin, D. J., et al. 2012, SoPh, 275, 17

Magyar, N., & Van Doorsselaere, T. 2016, A&A, 595, A81

Müller, D., Nicula, B., Felix, S., et al. 2017, A&A, 606, A10

Nakariakov, V. M., & Ofman, L. 2001, A&A, 372, L53

Nakariakov, V. M., Ofman, L., Deluca, E. E., Roberts, B., & Davila, J. M. 1999, Sci, 285, 862

Ofman, L., & Aschwanden, M. J. 2002, ApJL, 576, L153

Pascoe, D. J., Anfinogentov, S., Nisticò, G., Goddard, C. R., & Nakariakov, V. M. 2017, A&A, 600, A78

Pascoe, D. J., Goddard, C. R., Nisticò, G., Anfinogentov, S., & Nakariakov, V. M. 2016, A&A, 585, L6

Pascoe, D. J., Hood, A. W., De Moortel, I., & Wright, A. N. 2013, A&A, 551, A40

Reale, F. 2014, LRSP, 11, 4

Roberts, B., Edwin, P. M., & Benz, A. O. 1984, ApJ, 279, 857

Ruderman, M. S., & Roberts, B. 2002, ApJ, 577, 475

Ruderman, M. S., Verth, G., & Erdélyi, R. 2008, ApJ, 686, 694

Verwichte, E., Van Doorsselaere, T., White, R. S., & Antolin, P. 2013, A&A, 552, A138

Zajtsev, V. V., & Stepanov, A. V. 1975, IGAFS, 37, 3

Zimovets, I. V., & Nakariakov, V. M. 2015, A&A, 577, A4